Appl. Phys. A 87, 1–6 (2007)
DOI: 10.1007/s00339-006-3859-7

Applied Physics A
Materials Science & Processing

Invited paper

L.S. WANG[1,2]
D.B. BUCHHOLZ[1]
Y. LI[1]
J. LI[1]
C.Y. LEE[3]
H.T. CHIU[2]
R.P.H. CHANG[1,✉]

EELS plasmon studies of silver/carbon core/shell nanocables prepared by simple arc discharge

[1] Department of Materials Science and Engineering and Materials Research Institute, Northwestern University, 2220 Campus Drive, Evanston, Illinois 60208-3108 USA
[2] Department of Applied Chemistry, National Chiao Tung University, Hsinchu 30050, Taiwan, R.O.C.
[3] Materials Science Center, National Tsing Hua University, Hsinchu 30043, Taiwan, R.O.C.

Received: 5 December 2006/Accepted: 5 December 2006
Published online: 31 January 2007 • © Springer-Verlag 2007

ABSTRACT A method for the fabrication of large quantities of high quality silver nanocables encapsulated in carbon nanotubes (Ag@C) using a hydrogen arc is presented. A growth mechanism based on the generation of poly-aromatic hydrocarbons by the hydrogen arc is proposed. The size-dependent electronic structures of the resultant materials are investigated using electron energy loss spectroscopy (EELS). The surface plasmon and bulk-excitation character observed by EELS are discussed. As the diameter of Ag@C nanocable decreases, the surface and bulk plasmons of the silver core shift to lower energy and the peaks broaden. Measurements of electrical conductivity exhibits a liner current–voltage character with a conductivity of 0.5×10^4 S/cm for the nanocable structure.

PACS 81.05.Tp; 81.07.-b

1 Introduction

The discovery of one-dimensional (1D) nanomaterials has attracted much research attention [1–32]. Materials with a core/shell nanocable structure are of particular interest because of their potential for nanoelectronic and sensor applications. Recently, nanocable structures have been generated by the arc growth of carbon nanotubes (CNTs) in the presence of metal (M) or metal oxide (MO_x). The hollow core of CNTs can be filled to form a cable structure, M@C [33–37]. These include Mn@C, Cu@C and Ge@C. However, to our knowledge, preparation of Ag@C via this route has not been reported. A number of chemical methods have been developed to generate Ag@C nanocables [38–41]. Using chemical approaches, it is usually difficult to avoid impurities and the use of potentially hazardous reactants. Here, by employing the arc-discharge method, we report the first simple synthesis of high density and high purity Ag@C nanocables several micrometers in length.

We have also studied the plasmon resonances of these materials by electron energy loss spectroscopy (EELS) performed inside a transmission electron microscope. The high spatial resolution of this method allows us to study the electronic structure of individual Ag@C nanocables, while simultaneously obtaining size and microstructure information. Several surface-related features are observed in the energy loss spectra. The position and width of the plasmon peaks provide evidence for the influence of surface effects on charge carriers. In this paper, we report the effect of Ag@C nanocable diameter on plasmon excitations by EELS studies.

✉ Fax: +1-847-491-4181, E-mail: r-chang@northwestern.edu

2 Experimental

The arc system used in this study is described in detail elsewhere [42]. Briefly, the arc consists of two electrodes. The cathode is a solid 3/8 inch diameter randomly oriented graphite (ROG) rod. The anode is a cup-like structure fabricated from a 3/8 inch diameter ROG rod with a 3/16 inch diameter hole, 3/8 inch deep, in the center of the end facing the cathode. The hole, or cup, in the anode cup is filled with either tightly compacted carbon black (Alfa Aesar, 200 mesh, 99.99%) mixed with 10 ∼ 50 atomic percent of Ag powder, pure Ag powder (Inframat Advanced Materials, 150 nm, 99.95%), or a 3/16 inch diameter by 3/8 inch long Ag rod (alfa aesar, 99.99%). A 100 Amp DC arc is formed under a hydrogen atmosphere of 100 Torr. A potential of 20–30 V is maintained between the electrodes by adjusting the spacing between them, typically 0.5 to 0.7 inch A typical synthesis experiment lasts between 30 to 180 s. The powder deposits formed on the cathode side are collected and dispersed in ethanol using an ultrasonic bath. A lacy carbon grid is used to hold the specimens for electron microscopy observations.

Scanning electron microscopic (SEM) images were obtained using a Hitachi S-4500 field emission SEM (FESEM) operated at an acceleration voltage of 15 kV. Transmission electron microscopy (TEM), selected area electron diffraction (SAED), energy-dispersive X-ray spectroscopy (EDXS), electron energy loss spectroscopy (EELS) and scanning transmission electron microscopy (STEM) studies were performed using a JEOL 2100F FAST TEM working at 200 kV. The instrument is equipped with a Gatan slow scan charge-coupled device (CCD) camera, Oxford INCA EDXS and Gatan EELS attachments.

Nanocable devices for electrical characterization were fabricated by e-beam patterning of PMMA and lift-off of

Au/Pd metallization. To obtain isolated nanocables for patterning, arc deposits were dispersed in ethanol by ultrasonic agitation for 15 min. A drop of the nanocable-ethanol dispersion was transferred to a silicon dioxide on silicon substrate and allowed to dry. Electrical measurements of the nanocable were made by a two-terminal DC method at room temperature.

3 Results and discussion

Three types of silver containing anodes are used, 10% Ag powder mixed with carbon black, pure Ag powder and pure Ag rod. The color of the deposit on the ROG cathode changed from dark gray to light gray as the Ag content in the anode cup increased. Detailed characterization of the products will be discussed below. When Ag is not added to the anode-cup material, only black carbon-soot particles could be collected.

3.1 *Electron microscopic characterization*

The following discussion applies to structures formed in 100 Torr of H_2, 100 A current and a 25 V arc voltage. SEM images, Fig. 1, show the morphology of the products to be one-dimensional wire-like structures with lengths up to tens of micrometers. EDXS studies show they are comprised of C and Ag. As shown in Fig. 1b, many nanowires are terminated with nanoparticles, which, as determined by EDXS, also consist of C and Ag.

Also evident in Fig. 1b are portions of some wires that have unfilled cores. This suggests that the wires may have a core/shell type of cable-like structure. The diameter of the nanowire is dependent on the type of anode used: 30–145 nm, Fig. 1a, when 10% Ag powder mixed with carbon black is used; 160–240 nm, Fig. 1c, when pure Ag powder is used; and 350–580 nm, Fig. 1d, when pure Ag rod is used. The diameter of the structure increases as the Ag content of the anode increases.

TEM images of a sample prepared from 10% Ag powder mixed with carbon black are shown in Fig. 2. Figure 2a shows a 5 μm long nanowire with a diameter of 55 nm. The wire is connected to a 400 nm diameter nanoparticle. In Fig. 2b, a bundle of entangled nanowires comprised of C and a high quantity of Ag, as measured by EDXS, is shown. Evident in this image is the fact that a nanoparticle is often attached to one end of the nanowire. The shapes of the ends are round and smooth without sharp-cone caps. A straight uniform, nanowire with a diameter of 80 nm is shown in Fig. 2c. HRTEM from the area circled in Fig. 2c shows, in Fig. 2d–f, that the nanowire has a crystalline Ag core and a graphite shell ~ 6 nm in thickness. The distance between Ag atom layers is 0.204 nm, Fig. 2c. The SAED, Fig. 2f, shows reflections from both the crystalline Ag core and the graphite shell. The crystalline Ag core grows with the ⟨100⟩ direction preferentially oriented along the axis of the CNT. In the growth of thin films the preferred orientation is influenced by surface energy, interface energy and strain energy [43, 44]. Atomistic simulations of fcc Au nanowires predict that tensile surface-stress in a fcc ⟨100⟩ nanowire can cause it to reorient to fcc ⟨110⟩ [45]. Hence, an external compressive stress on the surface of our Ag

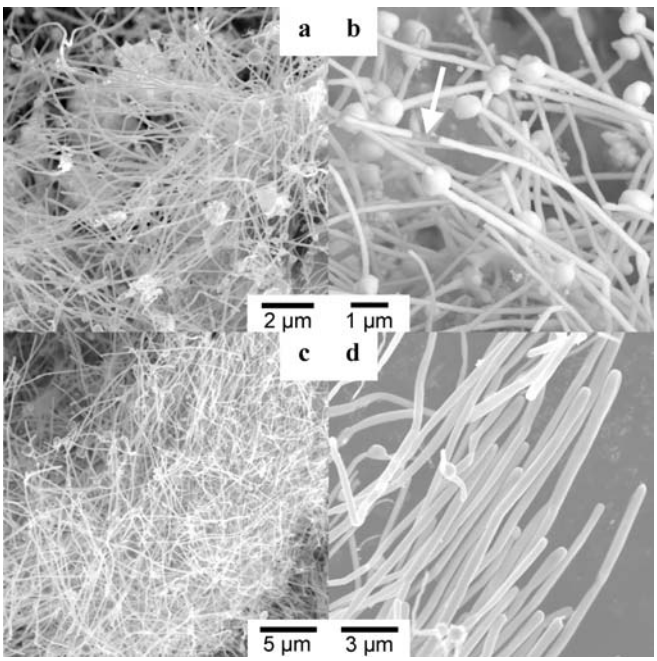

FIGURE 1 SEM images of arc-products synthesized with a 25 V potential between electrodes and an anode filling of (**a**) 10% Ag powered mixed with carbon black, (**b**) 10% Ag powered mixed with carbon black, high magnification image, (**c**) pure Ag powder, and (**d**) pure Ag rod

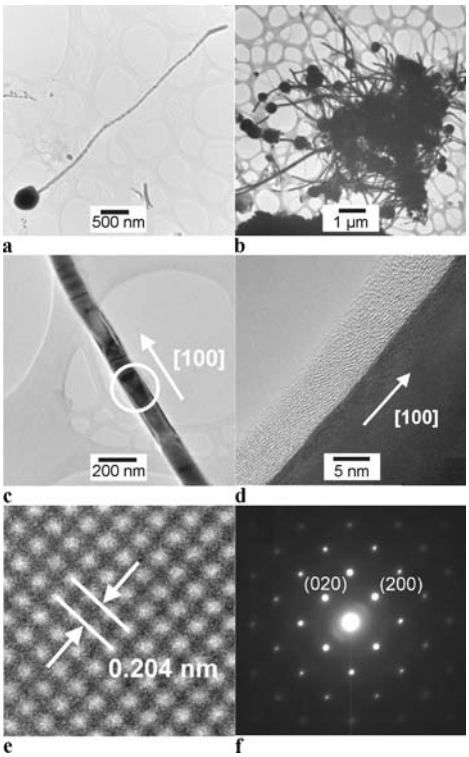

FIGURE 2 TEM images of arc-products synthesized with a 25 V potential between electrodes and an anode filling of 10% Ag powered mixed with carbon black. Low magnification TEM of (**a**) an individual 1-D Structure and (**b**) a product bundle. (**c**) TEM of nanocable region. The area circled in image (**c**) is shown as follows: (**d**) a HRTEM image of the sample showing a core-shell nanocable structure with a 6 mm graphite shell and an Ag core; (**e**) the Ag-core lattice image from (**c**); and (**f**) the corresponding SAED pattern indicating [100] growth direction

nanowire, perhaps from the graphite shell, may be the origin of our preferred ⟨100⟩ orientation.

Closer examination of the elemental composition and distribution confirms the Ag-core/C-shell structure of these nanocables. Figure 3a is a low magnification TEM image of a typical Ag@C nanocable. The light to dark contrast between the nanowire center and surface indicates a coaxial core/shell structure [46]. Figure 3b shows the EDXS analysis in nanobeam mode at the center of the nanocable and confirms that the nanocable is composed of mainly C and Ag.

In order to identify the coaxial cable-like structure further, the sample was examined by a high angle annular dark field (HAADF) image technique. This image is formed by collecting high-angle Rutherford forward-scattered electrons in z-contrast mode. Figure 3c shows a typical z-contrast image exhibiting a bright Ag crystalline core that diffracts electrons strongly. A focused electron beam, scanning along the route of the white line in Fig. 3c, confirms the elemental profile of the structure to be an Ag core surrounded by a C shell, Fig. 3d.

When the arc voltage is increased to 30 V, while still maintaining a 100 A current in 100 Torr H_2, Ag containing cables are produced in low quantity. The SEM image, Fig. 4a and the TEM images, Fig. 4b and c, show hollow core CNTs with little Ag incorporation. The SAED pattern from the area indicated in Fig. 4b shows reflections from only the graphite planes. The EDXS from the area marked in Fig. 4c only indicates the presence of C.

Isolated Ag particles, with sizes that range from 10 to hundreds of nanometers, are also observed, Fig. 4d. At an applied DC voltage of 30 V the arc is visibly more violent. The data suggests that under the more violent arc conditions the growth of the Ag@C cable structure is hampered.

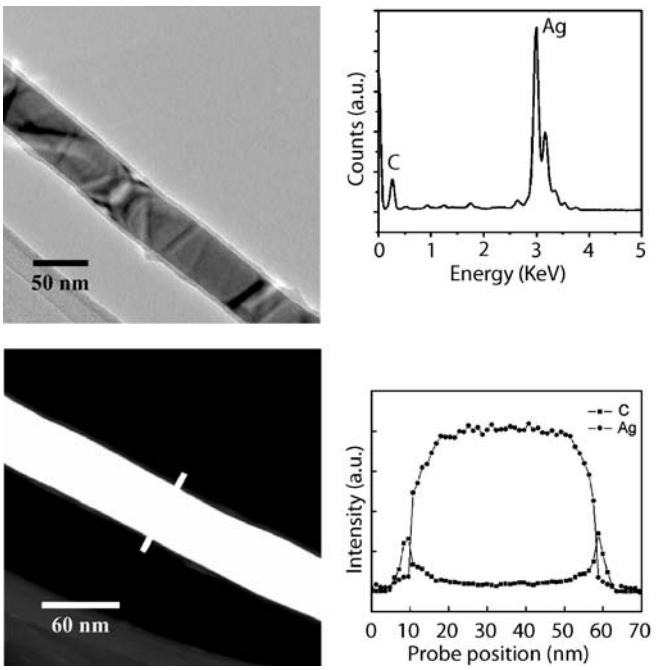

FIGURE 3 Nanocable region of arc products synthesized with a 25 V potential between the electrodes and an anode filling of 10% Ag powder mixed with carbon black: (**a**) TEM image, (**b**) EDXS, (**c**) HAADF z-contrast image and (**d**) element profile of Ag@C nanocable

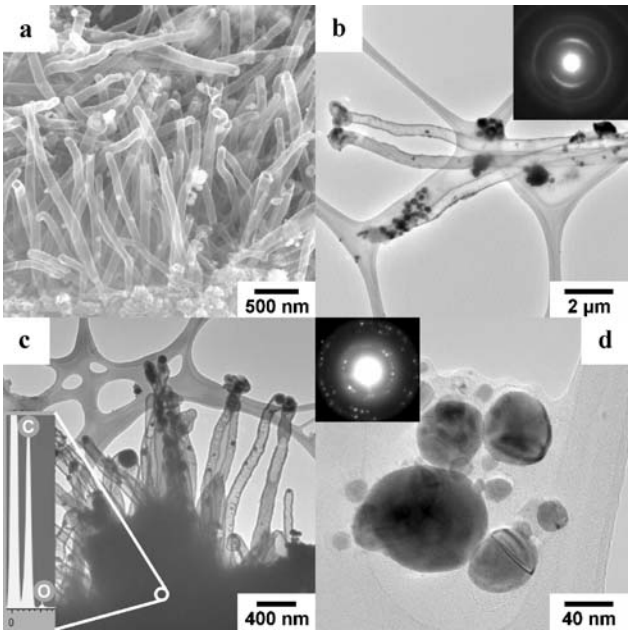

FIGURE 4 TEM images of arc-products synthesized with a 30 V potential between electrodes and an anode filling of 10% Ag powered mixed with carbon black. (**a**) SEM image of a hollow CNT bundle; most CNTs do not contain an Ag core, (**b**) TEM image and ED (*inset*) of dispersed CNTs. (**c**) TEM and EDXS of CNT bundle, and (**d**) TEM and ED (*inset*) of dispersed nanoparticles

3.2 *Proposed growth mechanism*

The mechanism proposed for the formation of carbon nanotubes filled with pure silver is similar to the mechanism we proposed for carbon nanotubes filled with copper [36] and germanium [37]. The formation of silver filled carbon nanotubes is only observed when we use a hydrogen arc, never when we use a helium arc. In earlier experiments on the effect of the reaction gas on the formation of carbon nanotubes and fullerenes, time-of-flight mass spectroscopy was performed on the soot produced by the carbon arc. When the soot from a hydrogen arc is compared to that from a helium arc it is found that no fullerenes are formed in the hydrogen arc and the quantity of poly aromatic hydrocarbon (PAH) molecules, resembling small graphitic sheets, is greatly increased. The presence of H radicals in a hydrogen arc allows PAH molecules to form [42]. The hydrogen arc generates small silver-clusters from the silver in the anode hole as well as the PAH molecules. The small silver clusters must interact with each other or with PAH molecules to reduce their surface energy and thus form the nucleus for nanotube growth. The CNT grows through the addition of PAH molecules and the silver nanowires by the addition of silver clusters.

The carbide formation-diffusion-decomposition and the carbon dissolution-diffusion-precipitation [47] mechanisms are not considered as favorable mechanisms for the growth of Ag@C structures. Silver forms no stable carbides and the solubility of carbon in silver is only 0.022 wt % (0.20 at. %) even at 1660 °C [48]. For a 50 nm diameter nanowire, such as the one pictured in Fig. 3a, a monolayer of graphite would represent a 5.2 at. % carbon structure. The overall structure in Fig. 3a, with a 6 nm thick CNT shell, represents a 51 at. % car-

bon structure. The lack of carbide formation and extremely limited solubility of carbon in silver are used to rule out these mechanisms. It should be pointed out that as the silver clusters cool, although very minor in quantity, the carbon dissolved in the silver precipitates out as graphite [48]. The graphite that precipitates does not in and of itself form the CNT, however, it could serve as a low energy point for the addition of PAH molecules from the arc.

Capillary filling is also not considered a favorable mechanism for the observed structure due to high surface tension of Ag, $\sim 900\,\mathrm{mN/m}$ at 1000 °C [49]. An upper limit for the capillary filling of MWCNTs appears to be on the order of 200 mN/m [50].

3.3 *Electron energy loss spectroscopic studies*

Surface plasmon phenomena and chemical composition of the nanowires are studied by EELS. A representative zero-loss EELS from the center of a Ag@C nanocable with a diameter of $\sim 100\,\mathrm{nm}$ is shown in Fig. 5a. Also visible are the Ag plasmon peaks below 40 eV and Ag-$N_{2,3}$ edges near 75 eV [51, 52]. Figure 5b displays a core-loss EELS with C-K and Ag-M edges at 284 eV and 396 eV, respectively [53, 54]. Features of the peaks are characteristic for electrons of graphite 1*s* to π^* and σ^* states as well as Ag 3*d* to vacuum [53]. Thus, the spectra clearly show that the nanocable is composed of Ag and graphitic C.

In order to study the surface plasmons of the Ag@C nanocables, high spatial resolution EELS analyses with 0.05 eV resolution is performed on subnanometer areas of the samples. For example, Fig. 6a is an EELS plasmon spectrum from the nanocable center shown in Fig. 5a. In the low-energy regime, five plasmon peaks are visible. Next to the zero loss peak, easily identifiable are the Ag plasmons at ~ 3.8 eV and ~ 8.3 eV, both of which are believed to be combined surface and bulk excitations [55]. In addition, three strong higher-energy loss peaks are found at 18.25, 25.55 and 33.85 eV. These are identified as the ionization edge of the bulk Ag features. The Ag spectrum is largely unaffected by the presence of the CNT. Figure 6b is the EELS plasmon spectrum of an Ag-free CNT shell obtained in this study. An important feature is the $\pi \rightarrow \pi^*$ transition peak at 6 eV [56]. The other is the $(\sigma + \pi)$ – plasmon, located at 23 eV. The $\pi \rightarrow \pi^*$ peak shape and intensity also provide an index to the amount of sp^2 carbon atoms. In this case, the spectrum suggests that the carbon shell contains a respectable quantity of sp^2 C.

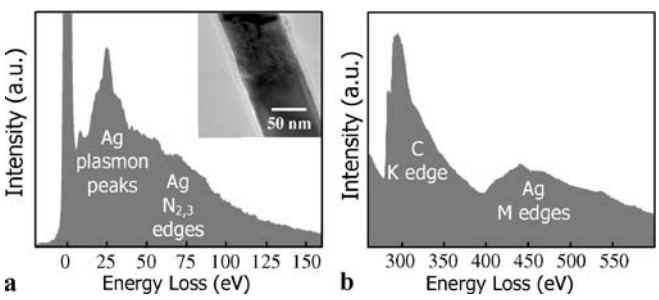

FIGURE 5 Typical EELS of a nanocable (**a**) zero-loss and (**b**) core-loss spectrum. The *inset* in (**a**) shows the nanocable region where EELS is taken

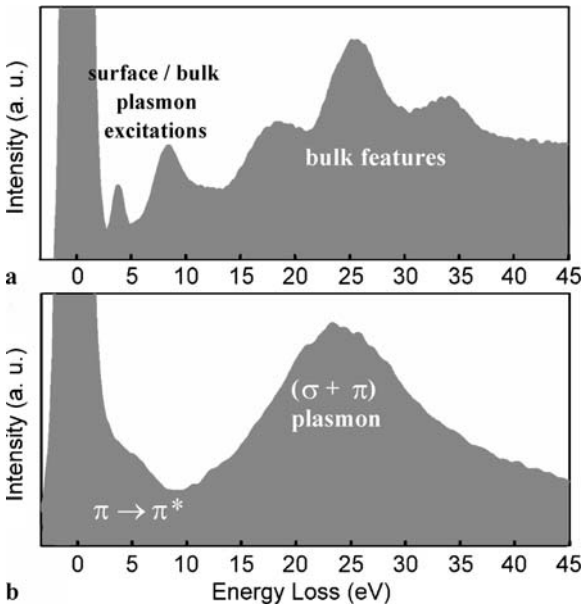

FIGURE 6 EELS plasmon spectra obtained from (**a**) an Ag@C nanocable and (**b**) an unfilled (Ag-free) CNT shell

The EELS plasmon spectra from Ag@C nanocables with diameters ranging from 42 to 145 nm were collected. In Fig. 7, energy loss of the plasmon peaks is plotted against the diameter of the Ag@C nanocables. The higher energy plasmon peak shifts from 8.0 eV to 5.5 eV as the diameter decreases from 145 to 42 nm. Also, within the same diameter variation range, the lower-energy plasmon-peak decrease from 3.8 to 2.9 eV. In metal nanowires, it is well-known that the surface-to-volume ratio becomes significant as the diameter shrinks. Energies of the plasmon peaks stay constant when the diameters are above 100 nm. However, when the cable diameter decreases below 100 nm, the peak location rapidly shifts to lower energy loss. These effects parallel surface plasmon energy shifts observed before for metal nanoparticles and nanowires [51, 57–59]. Also, the red shifts observed here agree with theoretical calculations using a dielectric theory model and a finite-difference time-domain (FDTD) method for surface plasmons in metallic particles

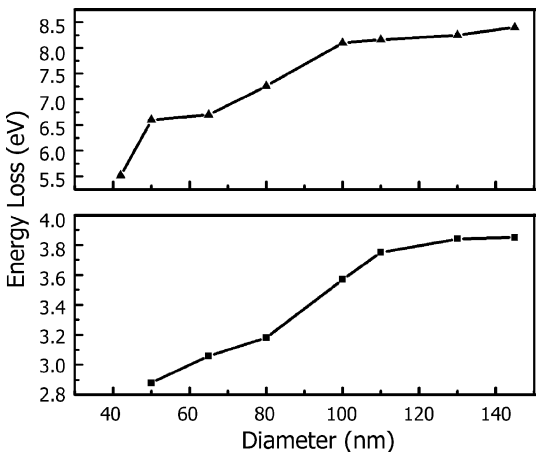

FIGURE 7 Energy loss verses Ag@C diameter for the two lowest energy surface/bulk plasmon excitations

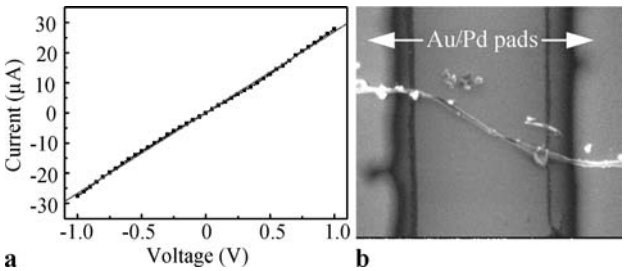

FIGURE 8 (**a**) Two point dc *I–V* curve for Ag@C nanocable. (**b**) SEM image of device; individual nanocable between two parallel Au/Pd electrodes

and nanowires [60, 61]. In summary, the energy shifts are due to size-related effects and variation in the surface-to-volume ratios.

A second size-related feature is also observed in the spectra. The Ag plasmon and excitation peaks broaden as the nanocable diameter decreases. This effect can be explained by increased scattering of oscillating electrons on the nanocable surface when the surface to volume ratio increases. The result is a decrease in relaxation time of the electrons which leads to broadening of the plasmon peaks [62].

3.4 *Electrical property study*

Measurements of the electrical conductivity for a typical Ag@C nanocable at room temperature were made using the two-point DC method. In Fig. 8, a linear *I–V* character of the Ag@C nanocable indicates an electrical conductivity of 0.5×10^4 S/cm. This value can be compared to 0.8×10^5 S/cm for an Ag nanowire [63] and 0.1×10^4 S/cm for multi-wall carbon nanotubes (MWCNTs) [64]. The conductivity of the Ag@C is somewhere between that of Ag and MWCNT. This can be explained in terms of an electrically continuous structure between the Ag-core and the C-shell. Although most of the electrons may pass through the graphite layers, some fraction of the electrons can penetrate through the graphite shell into the low resistance Ag metal core. This indicates that the Ag@C nanocables are electrically continuous. With proper modifications, they could serve as interconnects in nanoelectronic devices.

4 Conclusion

High crystal quality Ag-core/C-shell 1-D nanocables can be synthesized via a hydrogen arc method. The diameter of the Ag-core is dependent on the percentage of Ag present in the anode; the greater the percentage of Ag the larger the diameter of the Ag@C. The growth of the Ag@C structures is believed to proceed via a mechanism that requires a hydrogen arc to generate poly-aromatic hydrocarbons as the progenitor of the CNT. For Ag@C nanocables the EELS clearly shows the presence of both carbon and silver. In the low energy-loss region of the Ag@C nanocable EELS, the Ag plasmon peaks are clearly visible and largely unaffected by the CNT. The plasmon peaks shift toward lower energy as the diameters decrease. The peaks also broaden as the diameter decreases. The changes in the plasmon peaks with diameter can be attributed to size and surface-to-volume ratio effects.

ACKNOWLEDGEMENTS This work was supported by the MRSEC program of the National Science Foundation (DMR-0520513) at the Materials Research Center of Northwestern University and NASA (NCC 2-1363). We acknowledge the Northwestern University Atomic and Nanoscale Characterisation Center (NUANCE) for use of the JEOL 2100F FAST TEM. We are grateful to Dr. Jian-Guo Zheng for the TEM and EELS measurements in the NUANCE facility. We also thank Joel Horning making pattern by FIB. This work was also supported by the National Science council of Taiwan, Republic of China (NSC 94-2113-M-009 -013). L.-S. Wang thanks NSC for the Graduate Students Research Abroad Program.

REFERENCES

1 S. Iijima, Nature **354**, 56 (1991)
2 J. Hu, T.W. Odom, C.M. Lieber, Acc. Chem. Res. **32**, 435 (1999)
3 Y. Feldman, E. Wasserman, D.J. Srolovitt, R. Tenne, Science **267**, 222 (1995)
4 J. Kong, H.T. Soh, A.M. Cassell, C.F. Quate, H. Dai, Nature **385**, 878 (1998)
5 S.W. Chung, J.Y. Yu, J.R. Heath, Appl. Phys. Lett. **76**, 2068 (2000)
6 C. Dekker, Phys. Today **52**, 22 (1999)
7 S. Frank, P. Poncharal, Z.L. Wang, W.A. de Heer, Science **280**, 1744 (1998)
8 M.H. Huang, S. Mao, H. Feick, H. Yan, Y. Wu, H. Kind, E. Weber, R. Russo, P. Yang, Science **292**, 1897 (2001)
9 A. Bachtold, P. Hadley, T. Nakanishi, C. Dekker, Science **294**, 1317 (2001)
10 B.H. Hong, S.C. Bae, C.W. Lee, S. Jeong, K.S. Kim, Science **294**, 348 (2001)
11 B.H. Hong, J.Y. Lee, C.W. Lee, J.C. Kim, S.C. Bae, K.S. Kim, J. Am. Chem. Soc. **123**, 10 748 (2001)
12 C.H. Ye, G.W. Meng, Z. Jiang, G.Z. Wang, L.D. Zhang, J. Am. Chem. Soc. **124**, 15 180 (2002)
13 Z.L. Wang, Adv. Mater. **12**, 1295 (2000)
14 S.B. Suh, B.H. Hong, P. Tarakeshwar, S.J. Youn, S. Jeong, K.S. Kim, Phys. Rev. B **67**, 241 402(R) (2003)
15 Y.W. Wang, G.W. Meng, L.D. Zhang, C.H. Liang, J. Zhang, Chem. Mater. **14**, 1773 (2002)
16 T. Nautiyal, T.H. Rho, K.S. Kim, Phys. Rev. B **69**, 193 404 (2004)
17 Z. Zhang, X. Sun, M.S. Dresselhaus, J.Y. Ying, Phys. Rev. B **61**, 4850 (2000)
18 M. Bockrath, W. Liang, D. Bozovic, J.H. Hafner, C.M. Lieber, M. Tinkham, H. Park, Science **291**, 283 (2001)
19 F. Carmona, F. Barreau, P. Delhaes, R. Canet, J. Phys. Lett. **41**, L-531 (1980)
20 M.S. Dresselhaus, G. Dresselhaus, P.C. Eklund, *Science of Fullerenes and Carbon Nanotubes* (Academic, New York, 1996)
21 J.J. Davis, M.L.H. Green, H.A.O. Hill, Y.C. Leung, P.J. Sadler, J. Sloan, A.V. Xavier, S.C. Tsang, Inorg. Chim. Acta **272**, 261 (1997)
22 S.S. Wong, E. Joselevich, A.T. Woolley, C.C. Cheung, C.M. Lieber, Nature **394**, 52 (1998)
23 R.H. Baughman, C. Cui, A.A. Zakhidov, Z. Iqbal, J.N. Barisci, G.M. Spinks, G.G. Wallace, A. Mazzoldi, D. De Rossi, A.G. Rinzler, O. Jaschinski, S. Roth, M. Kertesz, Science **284**, 1340 (1999)
24 M.P. Mattson, R.C. Haddon, A.M. Rao, J. Mol. Neurosci. **14**, 175 (2000)
25 R. Martel, T. Schmidt, H.R. Shea, T. Hertel, P. Avouris, Appl. Phys. Lett. **73**, 2447 (1998)
26 Q.H. Wang, A.A. Setlur, J.M. Lauerhaas, J.Y. Dai, E.W. Seelig, R.P.H. Chang, Appl. Phys. Lett. **72**, 2912 (1998)
27 A.C. Dillon, K.M. Jones, T.A. Bekkedahl, C.H. Kinag, D.S. Bethune, M.J. Heben, Nature **386**, 377 (1997)
28 H.J. Dai, J.H. Hafner, A.G. Rinzler, D.T. Colbert, R.E. Smalley, Nature **384**, 147 (1996)
29 M.F. Yu, O. Lourie, M.J. Dyer, K. Moloni, T.F. Kelly, R.S. Ruoff, Science **287**, 637 (2000)
30 T.W. Ebbesen, P.M. Ajayan, Nature **358**, 220 (1992)
31 T. Guo, P. Nikolaev, A. Thess, D.T. Colbert, R.E. Smally, Chem. Phys. Lett. **243**, 49 (1995)
32 L. Kong, A.M. Cassell, H.J. Dai, Chem. Phys. Lett. **292**, 567 (1998)
33 P.M. Ajayan, C. Colliex, J.M. Lambert, P. Bernier, L. Barbedette, M. Tencé, O. Stephan, Phys. Rev. Lett. **72**, 1722 (1994)
34 C. Guerret-Piécourt, Y. Le Bouar, A. Loiseau, H. Pascard, Nature **372**, 761 (1994)
35 A. Loiseau, H. Pascard, Chem. Phys. Lett. **256**, 246 (1996)

36 A.A. Setlur, J.M. Lauerhaas, J.Y. Dai, R.P.H. Chang, Appl. Phys. Lett. **69**, 345 (1996)
37 J.Y. Dai, J.M. Lauerhaas, A.A. Setlur, R.P.H. Chang, Chem. Phys. Lett. **258**, 547 (1996)
38 D. Ugarte, A. Châtelain, W.A. de Heer, Science **274**, 1897 (1996)
39 J. Sloan, D.M. Wright, H.G. Woo, S. Bailey, G. Brown, A.P.E. York, K.S. Coleman, J.L. Hutchison, M.L.H. Green, Chem. Commun. 699 (1999)
40 A. Govindaraj, B.C. Satishkumar, M. Nath, C.N.R. Rao, Chem. Mater. **12**, 202 (2000)
41 X. Sun, Y. Li, Adv. Mater. **17**, 2626 (2005)
42 X.K. Wang, X.W. Lin, M. Mesleh, M.F. Jarrold, V.P. Dravid, J.B. Ketterson, R.P.H. Chang, J. Mater. Res. **10**, 1 (1995)
43 J.M.E. Harper, C. Cabral Jr., P.C. Andricacos, L. Gignac, I.C. Noyan, K.P. Rodbell, C.K.J. Hu, Appl. Phys. **86**, 2516 (1999)
44 G. Riveros, H. Gómez, A. Cortes, R.E. Marotti, E.A. Dalchiele, Appl. Phys. A **81**, 17 (2005)
45 J. Diao, K. Gall, M.L. Dunn, Phys. Rev. B **70**, 075423 (2004)
46 Y. Zhang, K. Suenaga, S. Colliex, S. Iijima, Science **281**, 973 (1998)
47 A. Oya, S. Otani, Carbon **17**, 131 (1979)
48 T.Y. Kosolapova, *Carbides: Properties, Production and Applications* (Plenium, New York, 1971)
49 R.C. Weast (Ed.), *CRC Handbook of Chemistry and Physics* (CRC, Boca Raton, Florida, 1981), p. F-23, 62nd edn.
50 E. Dujardin, T.W. Ebbesen, H. Hiura, K. Tanigaki, Science **265**, 1850 (1994)
51 H. Seiler, U. Hass, B. Ocker, K.H. Körtje, Faraday Discuss. **92**, 121 (1991)
52 D.J. Ding, H.M. Li, Q.R. Pu, Z.M. Zhang, Phys. Rev. B **66**, 085411 (2002)
53 C.C. Ann, O.L.K. Krivanek, R.P. Burgner, P.R. Swann, *EELS Atlas* (Gatan, Warrendale, 1983)
54 Z.S. Wronski, G.J. Carpenter, Carbon **44**, 1779 (2006)
55 D.J. Ding, H.M. Li, Q.R. Pu, Z.M. Zhang, Phys. Rev. B **66**, 085411 (2002)
56 Z.S. Wronski, G.J. Carpenter, Carbon **44**, 1779 (2006)
57 Y.W. Wang, B.H. Hong, J.Y. Lee, J.S. Kim, G.H. Kim, K.S. Kim, J. Phys. Chem. B **108**, 16723 (2004)
58 J. Wang, X. An, Q. Li, R.F. Egerton, Appl. Phys. Lett. **86**, 201911 (2005)
59 S. Hussain, R.K. Roy, A.K. Pal, J. Phys. D Appl. Phys. **38**, 900 (2005)
60 T. Stöckli, J.M. Bonard, P.A. Stadelmann, A. Châtelain, Z. Phys. D **40**, 425 (1997)
61 J.M. Oliva, S.K. Gray, Chem. Phys. Lett. **379**, 325 (2003)
62 B.W. Reed, J.M. Chen, N.C. MacDonald, J. Silcox, G.F. Bertsch, Phys. Rev. B **60**, 5641 (1999)
63 Y. Sun, Y. Yin, B.T. Mayer, T. Herricks, Y. Xia, Chem. Mater. **14**, 4736 (2002)
64 Q. Chen, S. Wang, L.M. Peng, Nanotechnology **17**, 1087 (2006)